ACS Chemical Neuroscience

Research Article

pubs.acs.org/chemneuro

Double Blockade of Glioma Cell Proliferation and Migration by Temozolomide Conjugated with NPPB, a Chloride Channel Blocker

Miri Park,[†,§] Chiman Song,[‡,§] Hojong Yoon,[‡] and Kee-Hyun Choi*[,†,‡]

[†]Department of Biological Chemistry, Korea University of Science and Technology, Daejeon 34113, Republic of Korea

[‡]Materials and Life Science Research Division, Korea Institute of Science and Technology, Seoul 02792, Republic of Korea

Supporting Information

ABSTRACT: Glioblastoma is the most common and aggressive primary malignant brain tumor. Temozolomide (TMZ), a chemotherapeutic agent combined with radiation therapy, is used as a standard treatment. The infiltrative nature of glioblastoma, however, interrupts effective treatment with TMZ and increases the tendency to relapse. Voltage-gated chloride channels have been identified as crucial regulators of glioma cell migration and invasion by mediating cell shape and volume change. Accordingly, chloride current inhibition by 5-nitro-2-(3-phenylpropylamino)-benzoate (NPPB), a chloride channel blocker, suppresses cell movement by diminishing the osmotic cell volume regulation. In this study, we developed a novel compound, TMZ conjugated with NPPB (TMZ-NPPB), as a potential anticancer drug. TMZ-NPPB blocked chloride currents in U373MG, a severely invasive human glioma cell line, and suppressed migration and invasion of U373MG cells. Moreover, TMZ-NPPB exhibited DNA modification activity similar to that of TMZ, and surprisingly showed remarkably enhanced cytotoxicity relative to TMZ by inducing apoptotic cell death via DNA damage. These findings indicate that TMZ-NPPB has a dual function in blocking both proliferation and migration of human glioma cells, thereby suggesting its potential to overcome challenges in current glioblastoma therapy.

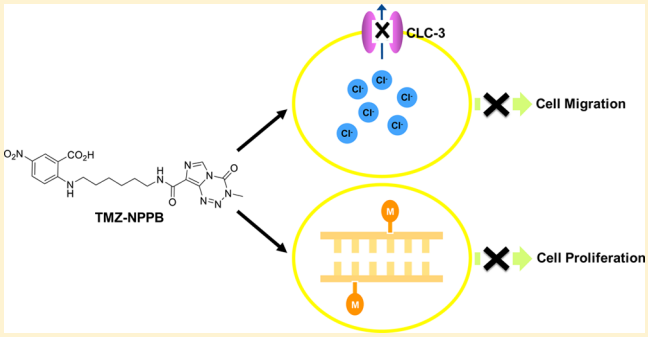

KEYWORDS: *Temozolomide, chloride channel blocker, NPPB, glioblastoma, voltage-gated chloride channel, migration, proliferation*

Glioblastoma is the most common and lethal primary brain tumor derived from glial progenitors of the central nervous system.[1,2] The prognosis of glioblastoma is poor due to its characteristics such as rapid proliferation and deregulated apoptosis. Glioblastoma has a tendency to readily spread to neighboring tissues, where it forms new satellites. Consequently, the survival time of glioblastoma patients generally does not exceed 1 year,[3,4] and overall 5 year survival rates remain less than 5%. Radiotherapy alone or concomitant radiotherapy with chemotherapy has been used as a standard treatment of glioblastoma.[5]

Temozolomide (TMZ) is an oral chemotherapeutic drug for glioblastoma, exerting its cytotoxicity to malignant cells by alkylating DNA. Under physiological pH, TMZ is hydrolyzed to 5-(3-methyltriazen-1-yl)imidazole-4-carboxamide (MTIC). MTIC is subsequently autodegraded to the methyldiazonium cation, which alkylates DNA at the *N*7 and *O*6 positions of guanine residues and at the *N*3 position of adenine residues.[6,7] Methylated purine bases of DNA induce cytotoxicity through failure of DNA repair systems. TMZ triggers DNA double-strand breaks, thereby arresting the G2/M cell cycle.[8,9] Currently, TMZ is the only available drug for glioblastoma. The infiltrative nature of glioblastoma, however, disrupts TMZ efficacy, resulting in high recurrence of glioblastoma.

Glioblastoma actively migrates through a narrow extracellular space via changes in cell volume and shape.[10] To modulate the cell volume, glioblastoma utilizes diverse ion channels including voltage-gated chloride channel 3 (CLC-3) and calcium-activated potassium channel 3.1 ($K_{ca}3.1$) that allow water secretion.[11,12] In particular, CLC-3 is 10-fold more expressed in glioblastoma than in nonmalignant brain tissues,[13] contributing to cell contraction by secreting chloride ions along with water.[14] Additionally, both CLC-3 knockdown using siRNA and chloride current inhibition by 5-nitro-2-(3-phenylpropylamino)-benzoate (NPPB), a non-specific chloride channel blocker, suppressed glioma cell migration and invasion.[15] These two lines of evidence further support the importance of CLC-3 in infiltration of glioblastoma.

On the basis of the evidence that the high expression of CLC-3 in glioblastoma plays a crucial role in glioblastoma migration, we developed TMZ conjugated with NPPB (TMZ-NPPB) as a dual-functional compound that inhibits glioma cell proliferation and migration simultaneously. We demonstrated that TMZ-NPPB functions both as a DNA alkylating agent and as a chloride channel blocker. Furthermore, we found that TMZ-NPPB not only effectively blocks migration of human glioma cells, but also shows enhanced cytotoxicity by inducing apoptotic cell death via DNA damage. Overall, this study suggests that

Received: June 30, 2015
Accepted: December 28, 2015
Published: December 29, 2015

DOI: 10.1021/acschemneuro.5b00178
ACS Chem. Neurosci. 2016, 7, 275−285

Scheme 1. Preparation of Temozolomide (TMZ) Conjugated with NPPB, a Chloride Channel Blocker (TMZ-NPPB) 8

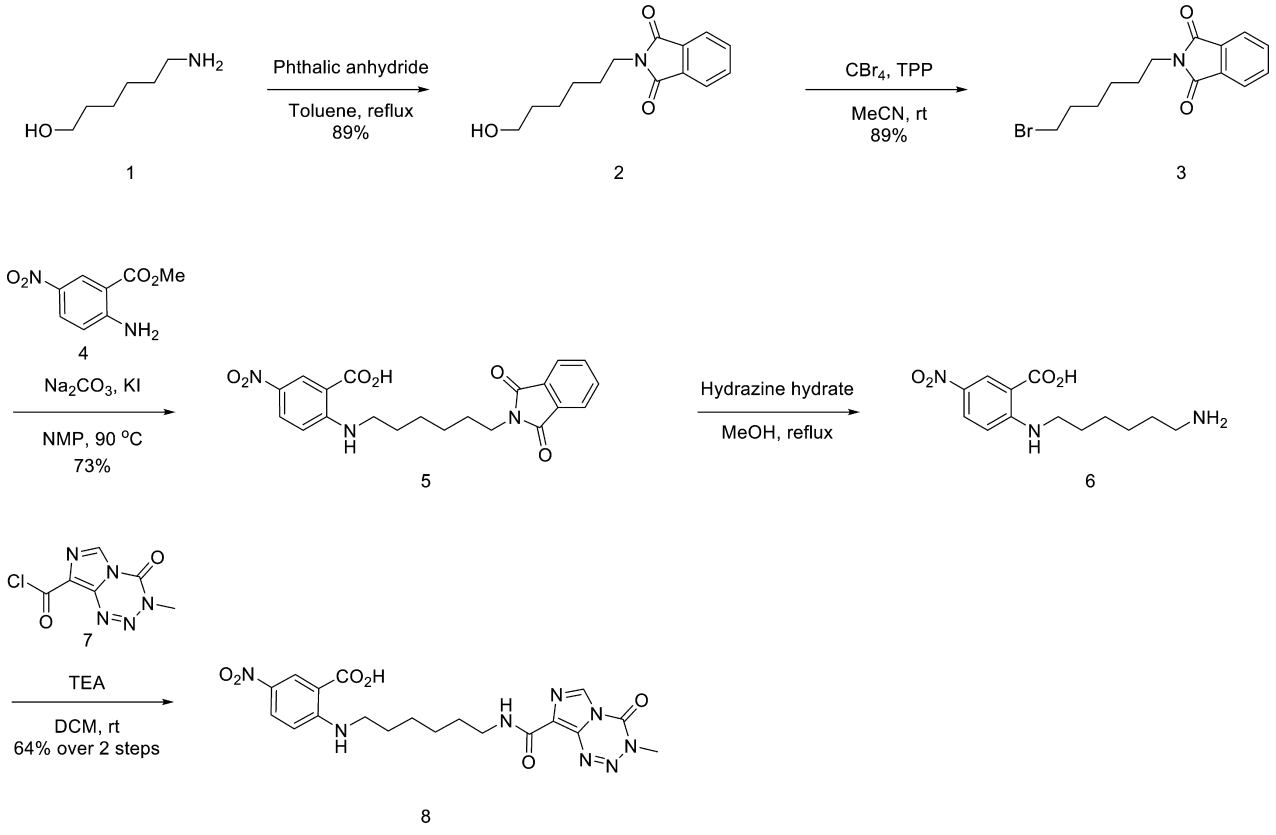

TMZ-NPPB could be developed as a novel anticancer drug with dual functions.

RESULTS AND DISCUSSION

TMZ Was Covalently Conjugated with NPPB. The synthesis of TMZ-NPPB commenced from commercially available 6-aminohexan-1-ol **1** (Scheme 1). Condensation of **1** with phthalic anhydride readily formed the phthalimide compound **2**, and subsequent Br-substitution using CBr_4/PPh_3 furnished bromo-substituted phthalimide **3**. Monoalkylation of methyl 2-amino-5-nitrobenzoate **4** with phthalimide **3** was successfully performed in the presence of Na_2CO_3 with a catalytic amount of KI. In the course of this alkylation reaction, the methyl ester functional group of **4** was hydrolyzed simultaneously. With the desired NPPB-linker compound **5**, we performed deprotection reaction of phthalimide with hydrazine. The resulted amine **6** was directly coupled with activated acid chloride of TMZ, yielding the desired TMZ conjugated with NPPB (TMZ-NPPB) **8**. TMZ exerts its antineoplastic effects after undergoing a chemical conversion in its six-membered ring.[7,16] NPPB blocks the chloride channel pore from the intracellular side via electrostatic interactions using its negatively charged carboxylic group.[17−19] Thus, a six-membered ring of TMZ and a carboxylic group of NPPB were not perturbed during conjugation.

TMZ-NPPB Maintains the Function of TMZ as a DNA Alkylating Agent. First, we verified that TMZ-NPPB maintains the original individual functions of TMZ and NPPB. To measure the activity of TMZ-NPPB as a DNA alkylating agent, the covalent DNA modification by TMZ-NPPB was detected in vitro. DNA fragments derived from the pBR322 vector were exposed to a test drug, and damaged DNA was amplified using a 5′-FAM-labeled primer. DNA polymerization was halted at methylated bases, generating smaller size bands in electrophoresis gel as shown in Figure 1A. The same fragmentation patterns were observed for TMZ- and TMZ-NPPB-treated DNA samples, indicating that covalent modification by TMZ and TMZ-NPPB occurred at identical positions. Given that consecutive guanine bases are susceptible for modification by TMZ,[20−22] the two major bands at the size of 80 and 100 bp are predicted to be from the guanine rich sequences around 110−112, 136−138, 160−165, and/or 172−174 bp as underlined in Figure 1A. The degree of DNA modification was quantified by densitometry analysis, revealing that TMZ-NPPB is as effective as TMZ for DNA methylation within experimental errors (Figure 1B). Overall, this result suggests that TMZ-NPPB functions like TMZ as a DNA alkylating agent, delivering a methyl group to DNA.

TMZ-NPPB Maintains the Function of NPPB as a Chloride Channel Blocker. Next, we tested whether TMZ-NPPB is capable of blocking chloride currents like NPPB. To examine the efficacy of TMZ-NPPB as a chloride channel blocker, we used U373MG, a highly invasive human glioma cell line.[23] We recorded voltage-dependent outward chloride currents in U373MG cells by applying voltage pulses from −60 to +120 mV in 20 mV increments using a whole-cell patch-clamp technique. Dose-dependent inhibition of chloride currents was observed with a 50% inhibitory concentration (IC_{50}) of 125 μM NPPB (Figure 2A), which is consistent with the IC_{50} of ∼100 μM previously reported for various cancer cells including human glioma cells.[24,25] TMZ-NPPB also blocked chloride currents comparably to NPPB in a concentration-dependent manner (Figure 2A). Calculated percent inhibitions of peak currents at +120 mV showed no statistical difference between NPPB and TMZ-NPPB (Figure 2B), implying that TMZ-NPPB retains the chloride channel blocking function of NPPB.

DOI: 10.1021/acschemneuro.5b00178
ACS Chem. Neurosci. 2016, 7, 275−285

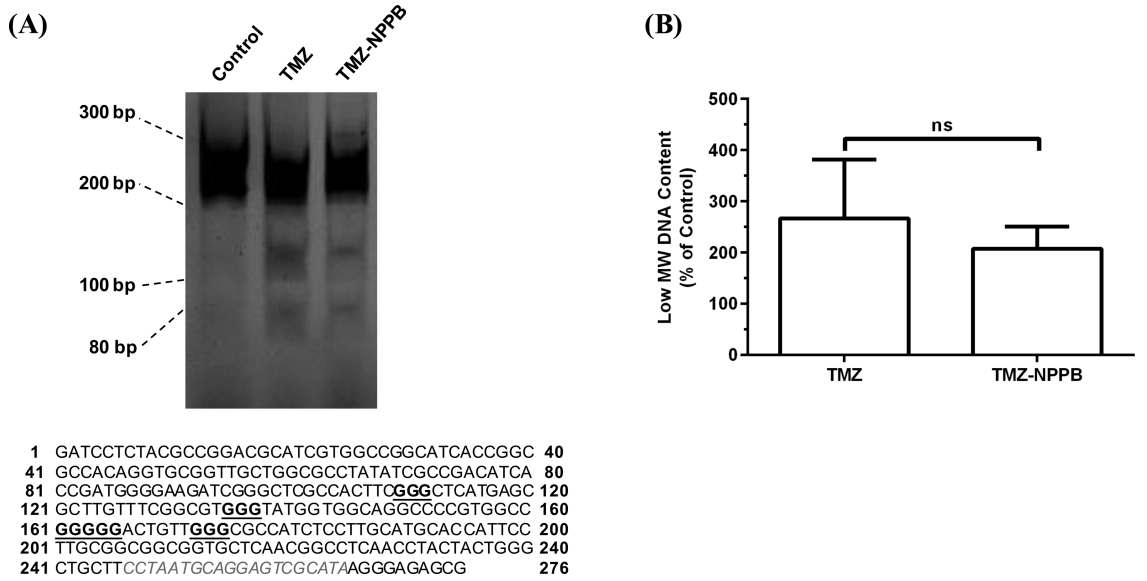

1 GATCCTCTACGCCGGACGCATCGTGGCCGGCATCACCGGC 40
41 GCCACAGGTGCGGTTGCTGGCGCCTATATCGCCGACATCA 80
81 CCGATGGGGAAGATCGGGCTCGCCACTTCGGGCTCATGAGC 120
121 GCTTGTTTCGGCGTGGGTATGGTGGCAGGCCCCGTGGCC 160
161 GGGGGACTGTTGGGCGCCATCTCCTTGCATGCACCATTCC 200
201 TTGCGGCGGCGGTGCTCAACGGCCTCAACCTACTACTGGG 240
241 CTGCTTCCTAATGCAGGAGTCGCATAAGGGAGAGCG 276

Figure 1. TMZ-NPPB maintains the function of TMZ as a DNA alkylating agent. (A) DNA fragments were shown in TMZ- and TMZ-NPPB-treated DNA samples, but not in untreated samples (Control). DNA templates were exposed to 1 mM of TMZ or TMZ-NPPB for 10 h. Nucleic acid sequence of the DNA template used for DNA fragmentation experiments is shown. Underlined guanines in bold indicate the putative methylation sites, and highlighted bases in italic gray are the primer sequence. (B) Densitometry analysis.

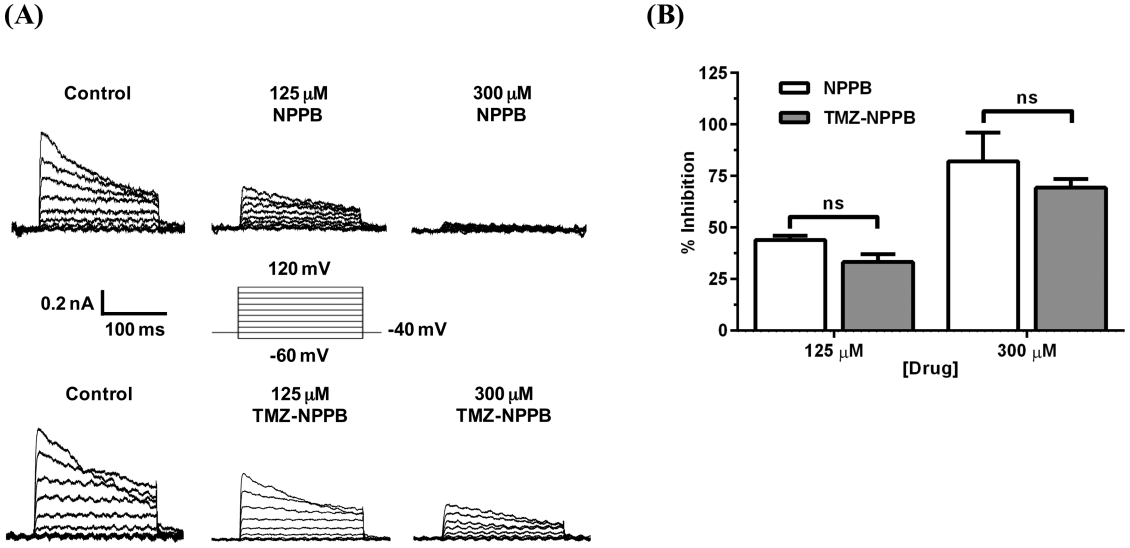

Figure 2. TMZ-NPPB maintains the function of NPPB as a chloride channel blocker. (A) Chloride currents of U373MG cells were decreased by NPPB and TMZ-NPPB in a concentration-dependent fashion. Voltage-dependent outward chloride currents were recorded using a whole-cell patch-clamp technique. (B) Differences in percent inhibitions between NPPB and TMZ-NPPB are not statistically significant.

TMZ-NPPB Suppresses U373MG Cell Proliferation by Inducing Apoptotic Cell Death. Since we verified the capability of TMZ-NPPB as a DNA alkylating agent in vitro, we measured effects of TMZ-NPPB on U373MG cell proliferation by MTT assays. The 50% growth inhibition concentration (GI_{50}) values of each test compound (TMZ, NPPB, TMZ-NPPB, and a mixture of TMZ and NPPB) were determined from its dose−response curve (Figure 3A) and summarized in Table 1. The mixture of TMZ and NPPB (TMZ + NPPB) is defined as equimolar concentrations of TMZ and NPPB. For example, 100 μM TMZ + NPPB refers to a combination of 100 μM TMZ and 100 μM NPPB. TMZ-NPPB has enhanced cytotoxic effects on human glioma cells compared to TMZ, with a GI_{50} value of 112 μM, about 10-fold lower than that of TMZ (GI_{50} of 1164 μM). We extended cell proliferation assays to other human glioma cell lines, U87MG and LN18, and observed similar results to those with U373MG cells; TMZ-NPPB exhibits approximately 10-fold enhanced efficacy relative to TMZ in both U87MG and LN18 cells (Figures S1 and Table 1). Although GI_{50} values of TMZ against human glioma cells determined in the present work are relatively high with broad distributions (Figure 3B), the reported values range from 10 to 1000 μM,[9,26−30] presumably due to differences in experimental conditions such as drug exposure time and/or the number of cells. Indeed, GI_{50} values of TMZ were reported to be less than 200 μM with 48−72 h drug exposure[9,26−28,30] while 24 h TMZ exposure provided GI_{50} values higher than 500 μM,[29] as observed in the present work. NPPB itself also shows cytotoxicity against glioma cells with a GI_{50} of approximately 500 μM, which is within the same order of magnitude of GI_{50} reported against

DOI: 10.1021/acschemneuro.5b00178
ACS Chem. Neurosci. 2016, 7, 275−285

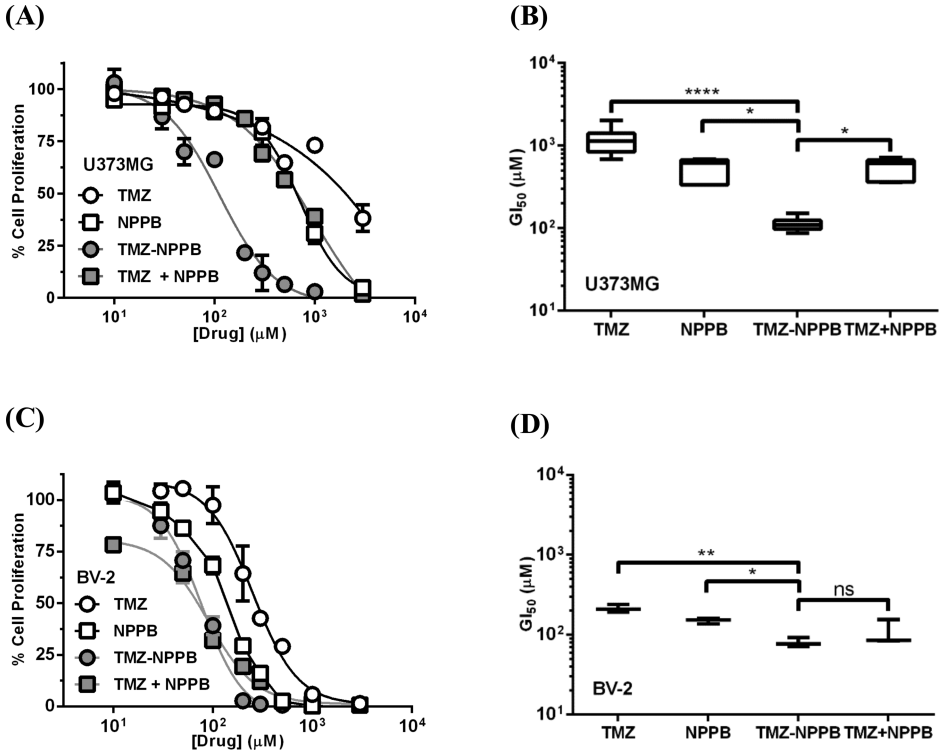

Figure 3. TMZ-NPPB shows enhanced efficacy as an antineoplastic drug compared to its mother compounds. Representative dose−response curves against U373MG cells (A) and BV-2 cells (C). Cells were exposed to various concentrations of test compounds for 24 h, and cell proliferation was measured using MTT assays. Dose−response curves were fitted to a Hill equation to obtain GI_{50} values. Box-and-whisker plots with minimum to maximum GI_{50} values for U373MG cells and BV-2 cells are presented in (B) and (D), repectively.

Table 1. GI_{50} Values against Glioma Cells (U373MG, U87MG, and LN18) and Microglial Cells (BV-2)

	TMZ (μM)	NPPB (μM)	TMZ-NPPB (μM)	TMZ + NPPB (μM)
U373MG	1164 ± 141	525 ± 78	112 ± 7	533 ± 72
U87MG	1259 ± 149	367 ± 29	130 ± 20	320 ± 18
LN18	1238 ± 247	381 ± 16	129 ± 10	375 ± 11
BV-2	241 ± 23	137 ± 7	77 ± 6	84 ± 8

nasopharyngeal carcinoma cells.[31,32] GI_{50} values of TMZ + NPPB against human glioma cells were similar to those of NPPB.

To investigate the selectivity of TMZ-NPPB toward glioma cells, we measured the antiproliferative activity of TMZ-NPPB against BV-2, a mouse microglial cell line. BV-2 cells were more susceptible to all test compounds than glioma cells (Figures 3C, D and Table 1). However, TMZ-NPPB showed improved selectivity compared to TMZ, NPPB, and TMZ + NPPB; the ratios of GI_{50} of TMZ-NPPB for glioma cells to GI_{50} for microglia cells were lower than those of other compounds (Table 2). This data indicates that relative selectivity of TMZ-NPPB for glioma cells over microglia cells is higher than that of TMZ although its absolute selectivity is lower for glioma cells than microglia cells.

Table 2. Selectivity Ratios of GI_{50} for Glioma Cells (U373MG, U87MG, and LN18) to GI_{50} for Microglial Cells (BV-2)

	TMZ	NPPB	TMZ-NPPB	TMZ + NPPB
U373MG	4.8	3.8	1.5	6.3
U87MG	5.2	2.7	1.7	3.8
LN18	5.1	2.8	1.7	4.5
BV-2	1	1	1	1

We further explored cell death pathways involving suppressed cell proliferation by TMZ-NPPB using flow cytometry analysis. Cells were incubated with 287 μM (GI_{80} of TMZ-NPPB) of each compound for 48 h to ensure sufficient cell death by TMZ-NPPB. Cell death was assessed by double-staining cells with FITC-annexin V, a cell death marker, and propidium iodide (PI), a necrosis marker. TMZ-NPPB facilitated cell death more than twice as much as TMZ or NPPB by inducing apoptosis, which is evidenced by the significantly higher percentage of gated cells in apoptosis stages (Figure 4). This observation is consistent with the previous finding that DNA damage induces cell death by apoptosis.[33] Overall, these data suggest that TMZ-NPPB inhibits glioma cell proliferation more effectively than TMZ via apoptosis pathways.

TMZ-NPPB Damages DNA More Effectively than TMZ. While in vitro efficacies of TMZ-NPPB and TMZ for covalent DNA modification are comparable, TMZ-NPPB is 10-fold more potent than TMZ as an antineoplastic agent against human glioma cells. The results from flow cytometry analysis showed that TMZ-NPPB induces more apoptotic cell death than TMZ, implying that TMZ-NPPB stimulates more DNA damage. To investigate this result further, we directly measured DNA damage of individual cells using single cell gel electrophoresis assays ("comet" assays). Whereas undamaged DNA retains nucleoid forms, damaged DNA relaxes its supercoiled structure, resulting in "comet" tails expanding toward the positively charged cathode on the electric field.[34,35] The comet assay was performed after exposure to 287 μM of each compound for 24 h. Representative images of comet assay show that TMZ-NPPB produced distinct comet tails, an indicator of DNA damage (Figure 5A). DNA damage was quantified by calculating percentage tail DNA (the intensity of comet tail relative to the head) and tail moment

DOI: 10.1021/acschemneuro.5b00178
ACS Chem. Neurosci. 2016, 7, 275−285

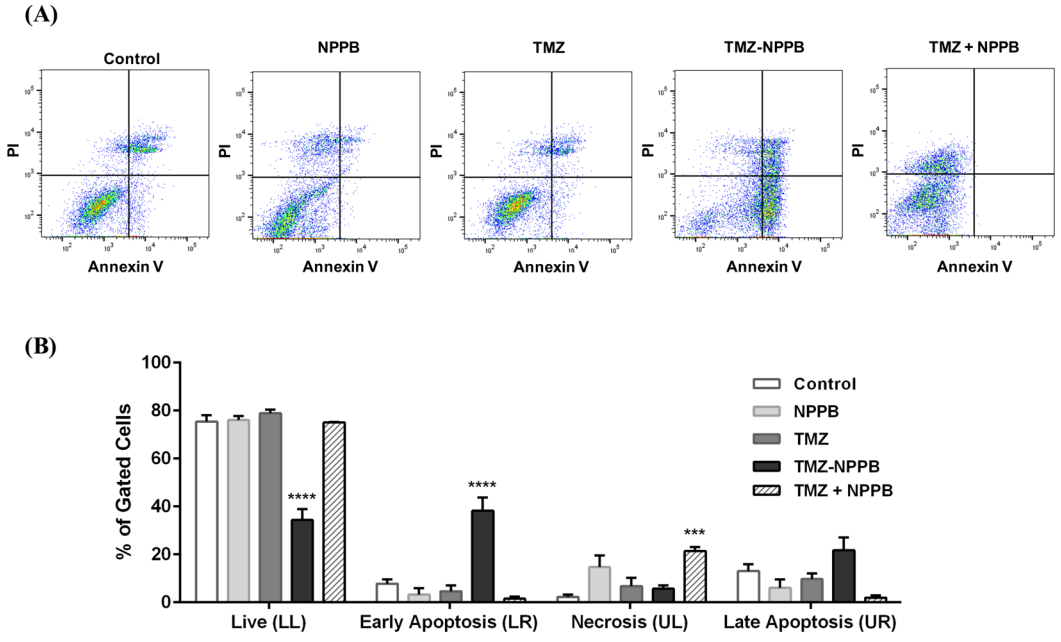

Figure 4. TMZ-NPPB induces apoptotic cell death as observed in flow cytometry analysis. (A) Cells were treated with 287 μM TMZ, NPPB, TMZ-NPPB, or TMZ + NPPB for 48 h, and then stained with FITC-annexin V and propidium iodide (PI). Untreated cells were used as a control. 10 000 cells per sample were analyzed. (B) Percentages of gated cells in each quadrant were represented as a bar graph. LL (live cells), LR (cells in early apoptosis), UL (cells in necrosis), and UR (cells in late apoptosis) are lower left, lower right, upper left, and upper right quadrants, respectively.

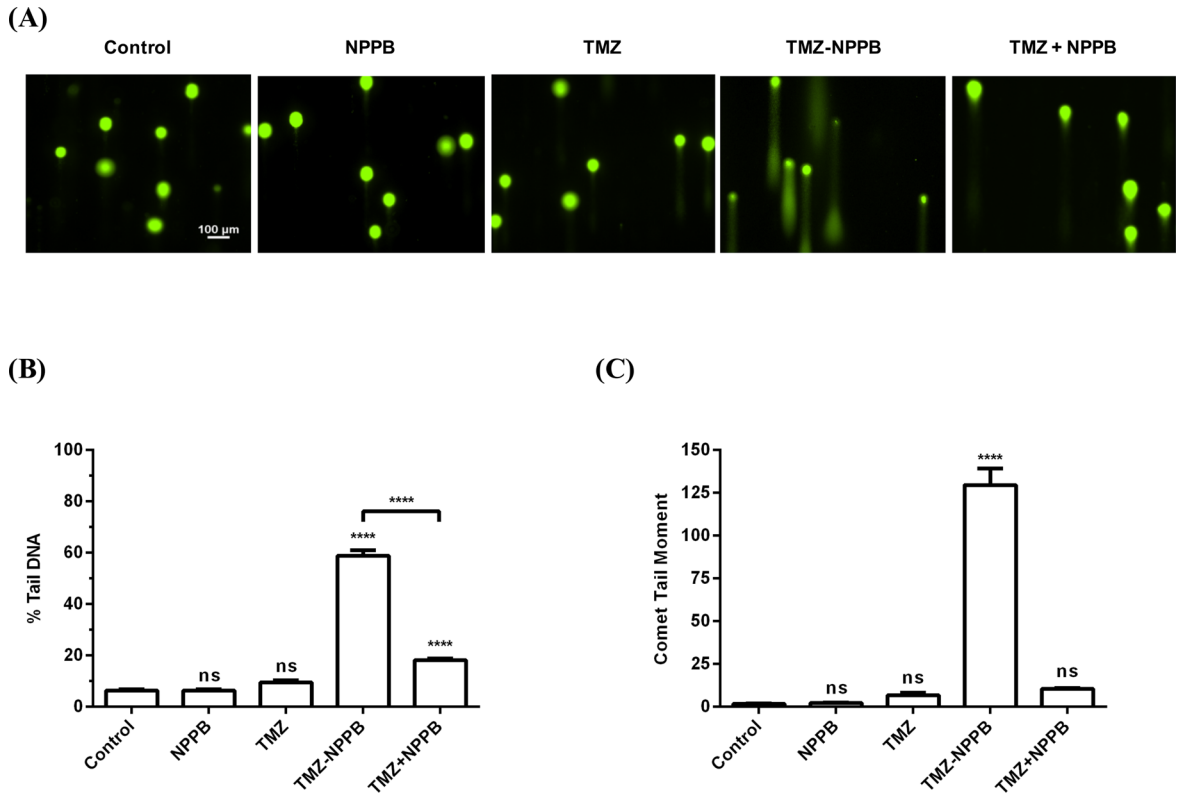

Figure 5. TMZ-NPPB enhances DNA double-strand break in U373MG cells analyzed by comet assays. Cells were treated with 287 μM TMZ, NPPB, TMZ-NPPB, or TMZ + NPPB for 24 h. Untreated cells were used as a control. (A) Representative images of DNA comets stained with SYBR green. Scale bar represents 100 μm. DNA lesion was quantified by calculating percentage tail DNA (B) and tail moment (C).

(product of the tail length and the fraction of DNA in the tail) as comet parameters.[36] TMZ-NPPB significantly increased percentage tail DNA and tail moment in U373MG cells compared to TMZ or NPPB (Figures 5B and 5C).

Cellular Uptake of TMZ-NPPB Is Comparable to That of TMZ. Although both TMZ and TMZ-NPPB cause cytotoxicity through DNA damage as the antiproliferative mechanism, TMZ-NPPB has 10-fold higher efficacy than TMZ against human

DOI: 10.1021/acschemneuro.5b00178
ACS Chem. Neurosci. 2016, 7, 275−285

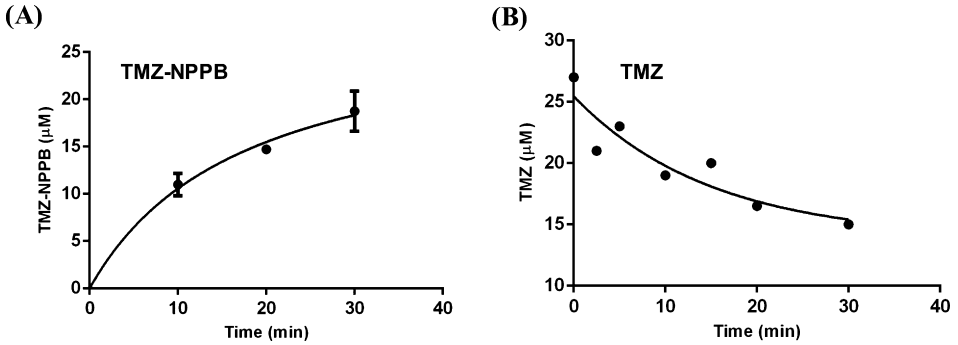

Figure 6. Cellular uptake of TMZ-NPPB and TMZ in glioblastoma cells. Time-course of concentration of intracellular TMZ-NPPB (A) and TMZ (B) adapted from ref 37.

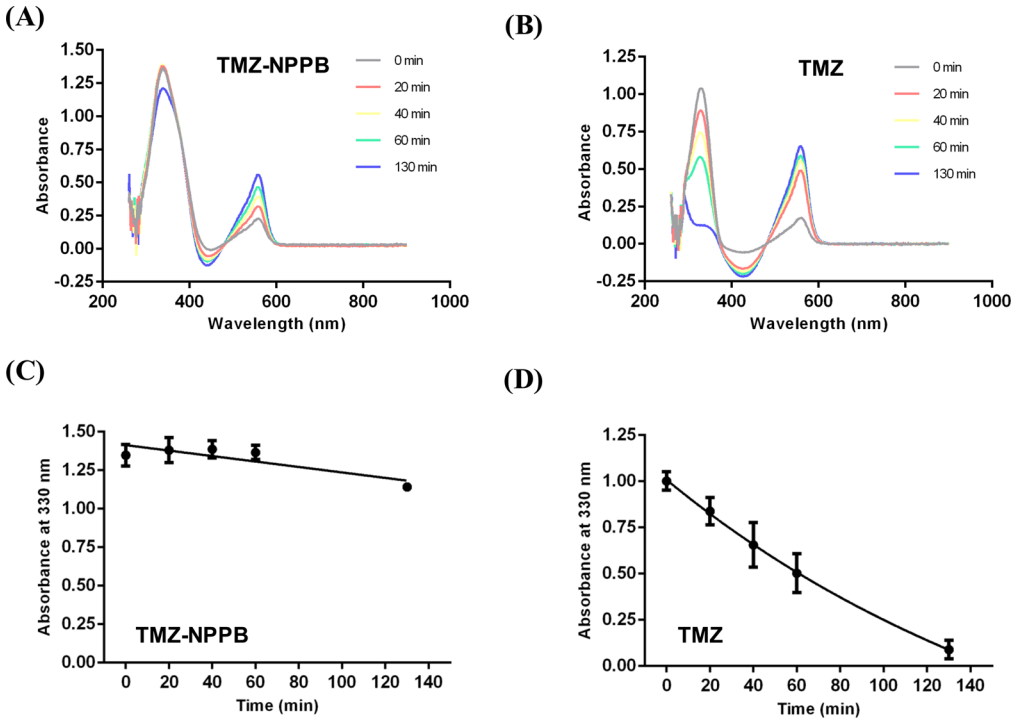

Figure 7. Stability of TMZ and TMZ-NPPB in cell culture media. Time-course of UV−vis absorption spectra of 100 μM TMZ-NPPB (A) and 100 μM TMZ (B). Time-course of absorbance at 330 nm of TMZ-NPPB (C) and TMZ (D).

glioma cells. We speculated that it might result from higher cellular uptake of TMZ-NPPB than TMZ. To test this hypothesis, we measured cellular import of TMZ-NPPB in U373MG cells using LC/MS/MS methods. Cellular uptake of TMZ-NPPB in U373MG cells gradually increased up to 19 μM at 30 min after cells were treated with 50 μM TMZ-NPPB (Figure 6A). Cellular uptake of TMZ was previously reported,[37] showing that intracellular TMZ continuously decreased to 15 μM at 30 min after cells were treated with 50 μM TMZ (Figure 6B adapted from ref 37). It is probably not only because TMZ is hydrolyzed to MTIC inside cells but also it is very unstable in neutral conditions.[38] Overall, cellular import of TMZ-NPPB was slightly higher than that of TMZ at 30 min after treatment. However, it is not sufficient to account for 10-fold higher efficacy of TMZ-NPPB. More plausible explanations would rather be the difference in uptake curve shapes; TMZ-NPPB uptake showed increase while TMZ uptake exhibited decease over time. It seems to be due to the difference in stability.

TMZ-NPPB Is More Stable than TMZ. Cellular activity of TMZ might be reduced due to its instability.[38] We, thus, tested stability of TMZ-NPPB and TMZ using UV−vis absorption spectra with the two distinctive peaks at 330 and 560 nm in Figure 7A and B, respectively. Amounts of TMZ-NPPB and TMZ were monitored by measuring absorbance at 330 nm as shown in Figure 7C and D, respectively. While we observed 80% of the initial of amount of TMZ-NPPB after 130 min incubation in cell culture media, TMZ was rapidly degraded, remaining only 12% after 130 min. These results imply that substantially higher stability of TMZ-NPPB would be a major factor of its increased antiproliferative effects compared to TMZ.

TMZ-NPPB Inhibits U373MG Cell Migration and Invasion. Voltage-gated chloride channels are required for glioblastoma cell migration because they mediate cell shape changes.[10,14] Thus, we tested whether inhibition of chloride currents in U373MG cells by TMZ-NPPB leads to suppression of cell migration. To monitor cell migration on two- and three-dimensional surfaces, we performed wound healing and matrigel invasion assays, respectively. Both assays were carried out at the GI_{50} values of each drug to allow equivalent cell proliferation conditions. For wound healing assays, images of scratched regions

DOI: 10.1021/acschemneuro.5b00178
ACS Chem. Neurosci. 2016, 7, 275−285

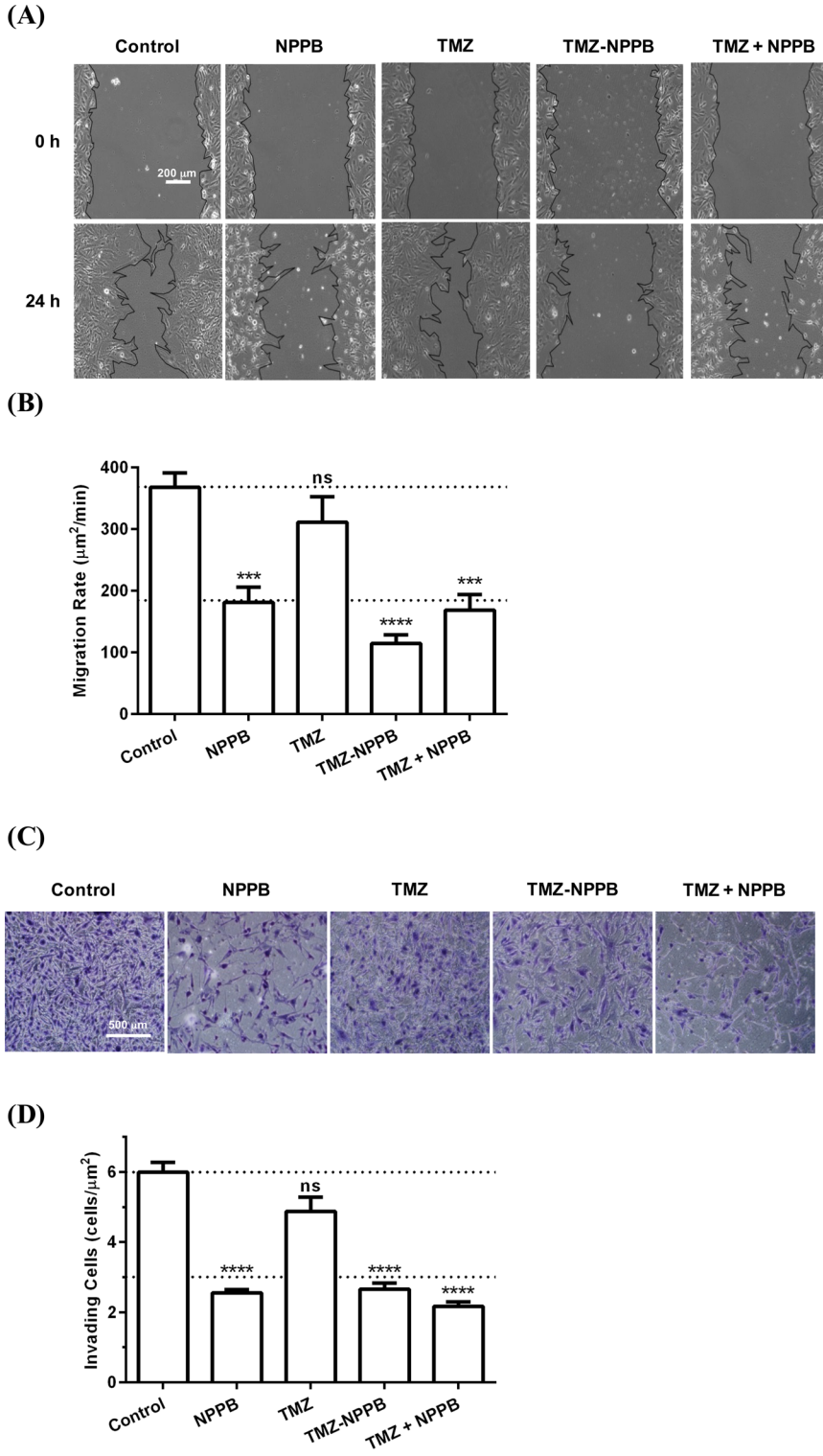

Figure 8. TMZ-NPPB suppresses migration and invasion of U373MG cells. (A) After scratching cell monolayers, cell migration was allowed for 24 h in the presence of each drug at its GI_{50} value. Scale bar represents 200 μm. (B) Migration rates were calculated from migration areas and time. (C) Cell invasion was allowed for 24 h in the presence of each drug at its GI_{50} value. Scale bar represents 500 μm. (D) Number of invading cells was quantified.

were taken before and after 24 h incubation (Figure 8A). Migration areas were determined as the difference between initial and final wounded regions, and migration rates were calculated by dividing migration areas by the incubation time, 24 h (Figure 8B). TMZ-NPPB decreased cell migration comparably to NPPB or TMZ + NPPB, while TMZ did not show any effects on cell migration. Effects of TMZ on glioma cell invasion have been controversial. Some reported that there are antimotility effects of TMZ,[39,40] while no effects of TMZ on cell invasion have been also reported,[41] as we observed in this work. Although different cell types and/or drug incubation conditions may partially contribute to the contradictory results, the fact that motility assays are affected by the number of cells would make the data analysis complicated, causing the mixed results. Indeed, reduced

DOI: 10.1021/acschemneuro.5b00178
ACS Chem. Neurosci. 2016, 7, 275−285

cell migration was observed only after prolonged incubation with TMZ, suggesting the influence of antiproliferative action of TMZ on cell motility assays via reduction of cell number.[41] We also observed the same results from matrigel invasion assays; TMZ-NPPB significantly reduced invasiveness of U373MG cells (Figure 8C and D). Taken together, these results suggest that TMZ-NPPB suppresses the infiltrative property of U373MG cells.

Conclusion and Future Directions. The strategy of conjugation has been attempted to improve pharmacological efficacy of existing drugs and/or to provide additional biological functions to them.[42,43] In particular, TMZ derivatives have been developed by covalently linking with other compounds to overcome various limits of TMZ for brain tumor therapy such as low efficacy against rapidly spreading glioma cells and nonselective targeting.[44−47] For example, TMZ conjugated with perillyl alcohol, another established chemotherapeutic agent, showed enhanced cytotoxic potency.[46] TMZ linked with targeting peptides facilitated cellular import and nuclear targeting.[45]

However, coupling a chloride channel blocker with TMZ has not previously been attempted. CLC-3 in glioma cell plasma membrane has been proposed as a crucial contributor to glioma cell migration.[14,15] Recent studies showed that calcium plays an important role in enhancing glioma cell migration through CLC-3.[12] Increased intracellular calcium activates CLC-3 via Ca^{2+}/calmodulin-dependent protein kinase II, which leads to the efflux of chloride ions and consequently induces cell contraction.[48] This process allows glioma cells to travel through extracellular space in the brain.

Our present work is the first study of conjugating TMZ with a chloride channel blocker to inhibit glioblastoma invasion. TMZ-NPPB suppresses glioblastoma cell proliferation and migration simultaneously as expected from the functions of its individual compounds. Interestingly, TMZ-NPPB showed dramatically improved cytotoxic efficacy against human glioma cells compared to TMZ by inducing apoptosis via direct DNA damage. It might result from higher cellular uptake of TMZ-NPPB than that of TMZ due to its stability and/or its NPPB moiety attracted by voltage-gated chloride channels highly expressed in glioma cells. Molecular mechanisms underlying enhanced cytotoxicity of TMZ-NPPB need to be elucidated further. For its clinical use, in vivo experiments using glioma animal models also need to be done to further confirm the biological functions of TMZ-NPPB observed on glioma cell lines. Nonetheless, these findings suggest that TMZ-NPPB could be developed as a potential therapeutic agent for glioblastoma with dual antitumor activities.

METHODS

Chemistry. All commercial reagents and solvents were purchased from commercial suppliers. All solvents were purified by standard techniques. All reactions were performed under N_2 atmosphere in flame-dried glassware. Reactions were monitored by TLC with 0.25 mm E. Merck precoated silica gel plates using a UV lamp, ninhydrin, or *p*-anisaldehyde stain. Purification of reaction products was carried out by silica gel column chromatography using Kieselgel 60 Art. 9385 (230−400 mesh). The purity of all compounds was over 95% based on their mass spectra obtained using the Waters LCMS system (2998 Photodiode Array Detector, 3100 Mass Detector, SFO System Fluidics Organizer, 2545 Binary Gradient Module, Reagent Manager, and 2767 Sample Manager) with SunFireTM C18 column (4.6 × 50 mm, 5 μm particle size). Solvent gradient was 60% (or 95%) A at 0 min and 1% A at 5 min; Solvent A = 0.035% TFA in H_2O; Solvent B = 0.035% TFA in MeOH; flow rate = 3.0 (or 2.5) mL/min. ^{1}H and ^{13}C NMR spectra were obtained using the Bruker 400-MHz FT-NMR spectrometer (400 MHz for ^{1}H and 100 MHz for ^{13}C). Standard abbreviations are used for denoting the signal multiplicities.

*2-(6-Hydroxyhexyl)isoindoline-1,3-dione (**2**).* To a solution of 6-aminohexan-1-ol **1** (1.11 g, 9.47 mmol) in toluene (30 mL) was added phthalic anhydride (1.41 g, 9.47 mmol), and then the mixture was refluxed with the Dean−Stark trap apparatus. After stirring for 2 h, the mixture was cooled to room temperature and concentrated under reduced pressure. Purification of the residue by column chromatography (50% EtOAc/hexane) yielded the target compound **2** (2.09 g, 89% yield) as colorless oil. ^{1}H NMR (400 MHz, $CDCl_3$) 7.85−7.81 (m, 2H), 7.72−7.69 (m, 2H), 3.68 (t, J = 7.2 Hz, 2H), 3.63 (q, J = 6.8 Hz, 2H), 1.69 (quint, J = 6.8 Hz, 2H), 1.56 (quint, J = 6.8 Hz, 2H), 1.45−1.34 (m, 4H).

*2-(6-Bromohexyl)isoindoline-1,3-dione (**3**).* To a solution of **2** (2.09 g, 8. 44 mmol) in acetonitrile (30 mL) was added carbon tetrabromide (3.6 g, 11 mmol) and triphenylphosphine (2.9 g, 11 mmol) at room temperature. After stirring for 2 h, the mixture was concentrated under reduced pressure. Purification of the residue by column chromatography (10% EtOAc/hexane) yielded the target compound **3** (2.33 g, 89% yield) as colorless oil. ^{1}H NMR (400 MHz, $CDCl_3$) 7.84−7.82 (m, 2H), 7.71−7.69 (m, 2H), 3.68 (t, J = 7.2 Hz, 2H), 3.38 (t, J = 6.8 Hz, 2H), 1.84 (quint, J = 6.8 Hz, 2H), 1.69 (quint, J = 6.8 Hz, 2H), 1.51−1.44 (m, 2H), 1.40−1.32 (m, 2H).

*2-((6-(1,3-Dioxoisoindolin-2-yl)hexyl)amino)-5-nitrobenzoic Acid (**5**).* To a solution of methyl 2-amino-5-nitrobenzoate **4** (1.35 g, 6.88 mmol) and 2-(6-bromohexyl)isoindoline-1,3-dione **3** (2.13 g, 6.88 mmol) in NMP (25 mL) was added sodium carbonate (1.45 g, 13.69 mmol) and potassium iodide (220 mg), and the reaction mixture was stirred at 90 °C for 36 h. After cooling to room temperature, the mixture was filtered through the Celite pad, and the organic layer was washed with water, and dried with $MgSO_4$. Purification of the residue by column chromatography (33% EtOAc/hexane) yielded the target compound **5** (2.64 g, 73% yield) as yellow solid. ^{1}H NMR (400 MHz, DMSO-d_6) 8.53 (d, J = 2.8 Hz, 1H), 8.47 (t, J = 2.0 Hz, 1H), 8.04 (dd, J = 2.8 Hz, 9.2 Hz, 1H), 7.83−7.77 (m, 6H), 6.85 (d, J = 9.2 Hz, 1H), 4.22 (t, J = 6.8 Hz, 2H), 3.55 (t, J = 6.8 Hz, 2H), 1.69 (quint, J = 6.8 Hz, 2H), 1.59 (quint, J = 6.8 Hz, 2H), 1.43−1.32 (m, 4H); ^{13}C NMR (100 MHz, DMSO-d_6) δ 167.90, 165.92, 155.81, 135.12, 134.29, 131.55, 128.77, 128.14, 122.91, 116.70, 107.60, 64.63, 37.23, 27.89, 27.81, 25.86, 25.01; LRMS (ESI) m/z 412.37 (M + H$^+$).

*2-((6-(3-Methyl-4-oxo-3,4-dihydroimidazo[5,1-d][1,2,3,5]-tetrazine-8-carboxamido)hexyl)amino)-5-nitrobenzoic Acid (**8**).* To a solution of **5** (1 g, 1.90 mmol) in methanol (100 mL) was added hydrazine hydrate (1.84 mL, 38 mmol), and the mixture was refluxed for 1.5 h. After the reaction was over, the reaction mixture was concentrated under reduced pressure to afford crude amine **6**. To a solution of amine **6** in CH_2Cl_2 (10 mL) was added triethylamine (0.8 mL, 5.7 mmol) and 3-methyl-4-oxo-3,4-dihydroimidazo[5,1-*d*][1,2,3,5]tetrazine-8-carbonyl chloride **7** (2.1 mmol) in CH_2Cl_2 (10 mL). After stirring for 1 h, the mixture was diluted with CH_2Cl_2, quenched with H_2O. The organic layer was washed with brine, dried over $MgSO_4$, filtered, and concentrated under reduced pressure. Recrystallization under the $CHCl_3$/hexane yielded the target compound **8** (557 mg, 64% yield, 2 steps) as yellow solid. ^{1}H NMR (400 MHz, DMSO-d_6) δ 8.81 (s, 1H), 8.57 (d, J = 2.8 Hz, 1H), 8.47 (t, J = 2.0 Hz, 1H), 8.07 (dd, J = 2.8 Hz, 9.2 Hz, 1H), 7.83 (s, 2H), 6.87 (d, J = 9.2 Hz, 1H), 4.26 (t, J = 6.8 Hz, 2H), 3.85 (s, 3H), 3.29 (q, J = 6.8 Hz, 2H), 1.73 (quint, J = 6.8 Hz, 2H), 1.56 (quint, J = 6.8 Hz, 2H), 1.45−1.37 (m, 4H); ^{13}C NMR (100 MHz, DMSO-d_6) δ 165.90, 159.49, 155.79, 139.16, 135.08, 134.27, 130.58, 128.79, 128.32, 128.12, 116.71, 107.58, 64.67, 38.37, 36.05, 29.02, 27.97, 26.00, 25.15; LRMS (ESI) m/z 459.64 (M + H$^+$).

Covalent DNA Modification. Covalent DNA modification was detected as previously described[20] with some modification. Briefly, DNA fragments between BamH*I* and Sal*I* restriction sites in pBR322 vector (New England Biolabs) were amplified using the forward primer 5′-GATCCTCTACGCCGGACGCA-3′ and the reverse primer 5′-CGCTCTCCCTTATGCGACTC-3′. The amplicon was purified by gel extraction using the Nucleospin Gel and PCR Clean-Up Kit (Macherey-Nagel, Germany). DNA fragments were treated with 1 mM TMZ (Sigma-Aldrich) or TMZ-NPPB in 50 μL of assay solution

DOI: 10.1021/acschemneuro.5b00178
ACS Chem. Neurosci. 2016, 7, 275−285

(25 mM triethanolamine and 1 mM EDTA at pH 7.2) for 10 h, and cleaned up using the MEGAquick-Spin Total Fragment DNA Purification Kit (Intron Biotechnology, Korea). The linear amplification was, then, performed using 5′-end fluorescein amidite (FAM)-labeled primer, 5′-TATGCGACTCCTGCATTAGG-3′ (Macrogen, Korea). Resulting DNA samples were purified and separated on 6% denaturing urea polyacrylamide gel. FAM-labeled DNA bands were detected at 494 nm on the Chemidoc MP Imaging System (Bio-Rad).

Cell Culture. The two human glioma cell lines, U373MG and U87MG, were obtained from Sigma-Aldrich. LN18 was purchased from American Tissue Culture Collection. BV-2, a mouse microglial cell line was kindly provided by Professor Kyoungho Suk (Kyungpook National University, Korea). These cells were used within 10 passages after receipt or resuscitation. The human glioma cells (U373MG also known as U251MG,[49] U87MG, and LN18) were cultured in Dulbecco's modified Eagle's medium (DMEM) supplemented with 10% (v/v) fetal bovine serum (FBS), 100 U/mL penicillin, and 100 μg/mL streptomycin (WelGene, Korea) at 37 °C in a humidified 5% CO_2 atmosphere. BV-2 cells were cultured in DMEM with 10% FBS, 100 U/mL penicillin, 100 μg/mL streptomycin, and 4 mM glutamic acid at 37 °C in a humidified 5% CO_2 atmosphere. Cells were passaged every 2 or 3 days.

Electrophysiology. Chloride currents of U373MG cells were recorded by a whole-cell patch-clamp technique using the EPC10 patch-clamp amplifier (HEKA Elektronik, Germany). Cells were seeded on polylysine-coated glass coverslips (12CIR-1; Fisher Scientific) and incubated for 4 h. Patch pipettes were pulled from thin-wall capillary glass tubing (G150T-3; Warner Instruments) using a micropipette puller (P-97; Sutter Instrument). Resistance of patch pipettes was ranged between 5 and 7 MΩ when filled with the internal solution. The external solution contains 130 mM NaCl, 5 mM KCl, 1 mM $CaCl_2$, 10.55 mM glucose, and 32.5 mM HEPES at pH 7.4 adjusted with NaOH. The internal solution contains 140 mM CsCl, 2 mM $MgCl_2$, 4.9 mM $CaCl_2$, 10 mM EGTA, and 10 mM HEPES at pH 7.2 adjusted with Tris base. The concentration of 4.9 mM calcium in the internal solution corresponds to intracellular free calcium of 180 nM, which enhances outward chloride currents by stimulating CLC-3.[12] Holding potential was −40 mV, and voltage pulses were applied from −60 to +120 mV in 20 mV increments. Electrophysiological data were acquired at 10 kHz and analyzed using PatchMaster software (HEKA Elektronik, Germany). For the inhibition experiments, 125 or 300 μM NPPB (Tocris Bioscience, U.K.) or TMZ-NPPB in the external solution was applied to the recording chamber. TMZ-NPPB was prepared by sonication for 10 min four times. Percent inhibitions were calculated using the maximum outward currents at +120 mV.

Cell Proliferation (MTT) Assay. Cells were seeded in the 96-well microtiter plate (Falcon) at a density of 5×10^3 cells per well and incubated at 37 °C for 24 h in a humidified 5% CO_2 atmosphere. After removing the culture medium, fresh media containing various concentrations of TMZ, NPPB, TMZ-NPPB, or a combination of TMZ and NPPB were added, and incubated for 24 h. Next, 100 μL of Thiazolyl blue tetrazolium bromide (Sigma-Aldrich) at 0.5 mg/mL was added to each well and incubated at 37 °C for 1 h. Cells were then dissolved in 100 μL of DMSO, and the absorbance was measured at 570 nm with FlexStation3 Microplate Reader (Molecular Devices). Concentration−response curves of each compound were fitted to a Hill equation to obtain GI_{50} and GI_{80} (50% and 80% growth inhibition concentrations, respectively) values.

Flow Cytometry Analysis. Flow cytometry analysis was performed using the Apoptosis Detection Kit with FITC-labeled annexin V and propidium iodide (PI) (BioLegend). U373MG cells were treated with 287 μM (GI_{80} of TMZ-NPPB) TMZ, NPPB, TMZ-NPPB, or a combination of TMZ and NPPB for 48 h. Untreated cells were used as a control. After 48 h incubation, cells were harvested, washed with phosphate-buffered saline (PBS), and resuspended in Annexin V Binding Buffer. Cells were stained with FITC-labeled annexin V for 15 min at room temperature in the dark, followed by addition of PI. Stained cells were immediately analyzed using BD FACS Canto II (BD Biosciences).

Comet Assay (Single Cell Gel Electrophoresis Assay). DNA damage in single individual cells was evaluated by the comet assay (Trevigen) using the manufacturer's protocol. In brief, U373MG cells were treated with 287 μM (GI_{80} of TMZ-NPPB) TMZ, NPPB, TMZ-NPPB, or a combination of TMZ and NPPB for 24 h. After incubation, cells were harvested and combined with LMAgarose. Then 50 μL of the mixture was immediately pipetted onto CometSlide. After gelling at 4 °C for 30 min in the dark, the slides were immersed in alkaline lysis solution (200 mM NaOH and 1 mM EDTA at pH > 13) and washed twice with Tris-borate EDTA buffer. Electrophoresis was carried out at 45 V for 5 min. The slides were washed twice with distilled water and then immersed in 70% ethanol. DNA was stained with SYBR green. Images were captured at 10× magnification using Nikon Eclipse *Ti* fluorescence microscopy (Nikon, Japan). Percentage tail DNA (the intensity of comet tail relative to the head) and tail moment (product of the tail length and the fraction of DNA in the tail) were calculated with 30 comets per sample using Comet Assay Software Project (CASP) image analysis software.

Cellular Uptake of TMZ-NPPB. U373MG cells were seeded onto 60 mm dishes (SPL Life Sciences Corp., Korea) at a density of 1×10^6 cells per dish, and cultured overnight. The cells were treated with 50 μM TMZ-NPPB for 10, 20, and 30 min, washed twice with cold PBS and then scraped in 200 μL of cold MeOH on ice. The cells were homogenized using a Dounce homogenizer. A volume of 20 μL of cell lysate was added to 60 μL of internal standard solution (0.1 μg/mL dacarbazine and 0.1% formic acid in MeOH). The mixture of cell lysate and internal standard solution was centrifuged at 20 000*g* for 10 min at 4 °C. The supernatant was analyzed by the LC/MS/MS method.

LC/MS/MS Analysis. The Agilent 1200 chromatographic system (Agilent Technologies) equipped with G1379B degasser, G1312B binary pump, G1367C autosampler, G136B column oven was used. Mass spectrometric analyses were carried out using the Agilent 6410 mass spectrometer (Agilent Technologies) with an electrospray ionization source. Chromatographic separation was performed using an analytical column (HECTOR-M C18, 150 × 2.0 mm, RStech Corp., Korea) with a gradient solvent system (Mobile Phase A: 0.5 mM ammonium formate (0.1% formic acid, v/v), B: acetonitrile). The detailed experimental parameters and conditions for LC/MS/MS analysis are described in the Supporting Information. The chromatographic system and the mass spectrometer were controlled by MassHunter workstation software Rev.B.03.01 (Agilent Technologies). Quantitative analysis was carried out using a standard calibration curve.

Ultraviolet−Visible (UV−vis) Absorption Spectra. A concentration of 100 μM TMZ or TMZ-NPPB was incubated in cell culture media. Absorption spectra were obtained at various time points (0, 20, 40, 60, and 130 min) using DU-650, a UV−vis spectrophotometer (Beckman Coulter). Absorbance at 330 nm as a function of time was fitted with a one phase exponential decay equation:

$$A_t = (A_0 - A_i)^{-kt} + A_i$$

where A_t is the absorbance at a given time, A_0 is the initial absorbance, A_i is the absorbance at infinite time, k is the rate constant, and t is time.

Wound Healing Assay. U373MG cells were seeded in 6-well plates (Nunc) coated with polylysine at a density of 5×10^5 cells per well and incubated overnight. Cell monolayers were wounded using a 10 μL pipet tip and then washed with PBS twice to remove the detached cells. Cells were incubated with a test compound at its GI_{50} for 24 h. The images of scratched regions were taken before and after 24 h incubation, and migration rates were calculated from migration areas determined using ImageJ software (National Institutes of Health).

Matrigel Invasion Assay. Matrigel invasion chambers with a pore size of 8.0 μm in a 24-well plate (BioCoat/Corning) were rehydrated. U373MG cell suspension in fresh medium containing a test compound at its GI_{50} was added to the chamber at a density of 1×10^5 cells per well. After 24 h incubation at 37 °C, cells were fixed with formaldehyde and methanol, and stained with trypan blue (Invitrogen). After removing the remaining cells on the upper surface of the membrane, the number of invading cells was counted using ImageJ software.

DOI: 10.1021/acschemneuro.5b00178
ACS Chem. Neurosci. 2016, 7, 275−285

Data Analysis. All data are presented as the mean ± SEM. The significance of observed differences was evaluated by an unpaired *t* test using Prism 6 (GraphPad). A *P* value of <0.05 was considered statistically significant.

■ ASSOCIATED CONTENT

Supporting Information

The Supporting Information is available free of charge on the ACS Publications website at DOI: 10.1021/acschemneuro.5b00178.

Experimental parameters and conditions for LC/MS/MS analysis, and dose−response curves of U87MG and LN-18 cells (PDF)

■ AUTHOR INFORMATION

Corresponding Author

*Mailing address: Hwarangno 14-gil 5, Seongbuk-gu, Seoul 02792, Republic of Korea. Tel: +82-2-958-5930. E-mail: keehyun@kist.re.kr; keehyun.choi@gmail.com.

Author Contributions

§M.P. and C.S. contributed equally to this work. K.-H.C. conceived of the study. M.P., C.S., and K.-H.C. designed the experiments. M.P. and C.S. conducted the experiments. H.Y. synthesized the compound. M.P., C.S., and K.-H.C. analyzed the data, and wrote and edited the manuscript.

Funding

This research was supported by the funds from the Korea Institute of Science and Technology (Grant Number 2E25340).

Notes

The authors declare no competing financial interest.

■ ACKNOWLEDGMENTS

We thank Ms. Shulki Park and Ms. Heeyoung Ju for their technical assistance. We also thank Dr. Eleanor Fraser at UCSF for her thorough proofreading.

■ REFERENCES

(1) Furnari, F. B., Fenton, T., Bachoo, R. M., Mukasa, A., Stommel, J. M., Stegh, A., Hahn, W. C., Ligon, K. L., Louis, D. N., Brennan, C., Chin, L., DePinho, R. A., and Cavenee, W. K. (2007) Malignant astrocytic glioma: genetics, biology, and paths to treatment. *Genes Dev. 21*, 2683−2710.

(2) Louis, D. N. (2006) Molecular pathology of malignant gliomas. *Annu. Rev. Pathol.: Mech. Dis. 1*, 97−117.

(3) Chen, J., McKay, R. M., and Parada, L. F. (2012) Malignant glioma: lessons from genomics, mouse models, and stem cells. *Cell 149*, 36−47.

(4) Wen, P. Y., and Kesari, S. (2008) Malignant gliomas in adults. *N. Engl. J. Med. 359*, 492−507.

(5) Stupp, R., Mason, W. P., van den Bent, M. J., Weller, M., Fisher, B., Taphoorn, M. J., Belanger, K., Brandes, A. A., Marosi, C., Bogdahn, U., Curschmann, J., Janzer, R. C., Ludwin, S. K., Gorlia, T., Allgeier, A., Lacombe, D., Cairncross, J. G., Eisenhauer, E., and Mirimanoff, R. O. (2005) Radiotherapy plus concomitant and adjuvant Temozolomide for glioblastoma. *N. Engl. J. Med. 352*, 987−996.

(6) Zhang, J., Stevens, M. F., and Bradshaw, T. D. (2012) Temozolomide: mechanisms of action, repair and resistance. *Curr. Mol. Pharmacol. 5*, 102−114.

(7) Friedman, H. S., Kerby, T., and Calvert, H. (2000) Temozolomide and treatment of malignant glioma. *Clin. Cancer Res. 6*, 2585−2597.

(8) Hirose, Y., Berger, M. S., and Pieper, R. O. (2001) p53 effects both the duration of G(2)/M arrest and the fate of Temozolomide-treated human glioblastoma cells. *Cancer Res. 61*, 1957−1963.

(9) Kanzawa, T., Germano, I. M., Komata, T., Ito, H., Kondo, Y., and Kondo, S. (2004) Role of autophagy in Temozolomide-induced cytotoxicity for malignant glioma cells. *Cell Death Differ. 11*, 448−457.

(10) Cuddapah, V. A., Robel, S., Watkins, S., and Sontheimer, H. (2014) A neurocentric perspective on glioma invasion. *Nat. Rev. Neurosci. 15*, 455−465.

(11) Molenaar, R. J. (2011) Ion channels in glioblastoma. *ISRN Neurol. 2011*, 590249.

(12) Cuddapah, V. A., Turner, K. L., Seifert, S., and Sontheimer, H. (2013) Bradykinin-induced chemotaxis of human gliomas requires the activation of KCa3.1 and ClC-3. *J. Neurosci. 33*, 1427−1440.

(13) Cuddapah, V. A., and Sontheimer, H. (2010) Molecular interaction and functional regulation of ClC-3 by Ca2+/calmodulin-dependent protein kinase II (CaMKII) in human malignant glioma. *J. Biol. Chem. 285*, 11188−11196.

(14) Olsen, M. L., Schade, S., Lyons, S. A., Amaral, M. D., and Sontheimer, H. (2003) Expression of voltage-gated chloride channels in human glioma cells. *J. Neurosci. 23*, 5572−5582.

(15) Lui, V. C. H., Lung, S. S. S., Pu, J. K. S., Hung, K. N., and Leung, G. K. K. (2010) Invasion of Human Glioma Cells Is Regulated by Multiple Chloride Channels Including ClC-3. *Anticancer Res. 30*, 4515−4524.

(16) Denny, B. J., Wheelhouse, R. T., Stevens, M. F., Tsang, L. L., and Slack, J. A. (1994) NMR and molecular modeling investigation of the mechanism of activation of the antitumor drug Temozolomide and its interaction with DNA. *Biochemistry 33*, 9045−9051.

(17) Linsdell, P. (2014) Cystic fibrosis transmembrane conductance regulator chloride channel blockers: Pharmacological, biophysical and physiological relevance. *World J. Biol. Chem. 5*, 26−39.

(18) St. Aubin, C. N., Zhou, J. J., and Linsdell, P. (2007) Identification of a second blocker binding site at the cytoplasmic mouth of the cystic fibrosis transmembrane conductance regulator chloride channel pore. *Mol. Pharmacol. 71*, 1360−1368.

(19) Walsh, K. B., Long, K. J., and Shen, X. F. (1999) Structural and ionic determinants of 5-nitro-2-(3-phenylpropylamino)-benzoic acid block of the CFTR chloride channel. *Br. J. Pharmacol. 127*, 369−376.

(20) Ponti, M., Forrow, S. M., Souhami, R. L., D'Incalci, M., and Hartley, J. A. (1991) Measurement of the sequence specificity of covalent DNA modification by antineoplastic agents using Taq DNA polymerase. *Nucleic Acids Res. 19*, 2929−2933.

(21) Moody, C. L., and Wheelhouse, R. T. (2014) The medicinal chemistry of imidazotetrazine prodrugs. *Pharmaceuticals 7*, 797−838.

(22) Arrowsmith, J., Jennings, S. A., Langnel, D. A. F., Wheelhouse, R. T., and Stevens, M. F. G. (2000) Antitumour imidazotetrazines. Part 39. Synthesis of bis(imidazotetrazine)s with saturated spacer groups. *J. Chem. Soc., Perkin Trans. 1*, 4432−4438.

(23) Chahal, M., Abdulkarim, B., Xu, Y., Guiot, M. C., Easaw, J. C., Stifani, N., and Sabri, S. (2012) O6-Methylguanine-DNA methyltransferase is a novel negative effector of invasion in glioblastoma multiforme. *Mol. Cancer Ther. 11*, 2440−2450.

(24) Ransom, C. B., O'Neal, J. T., and Sontheimer, H. (2001) Volume-activated chloride currents contribute to the resting conductance and invasive migration of human glioma cells. *J. Neurosci. 21*, 7674−7683.

(25) Mao, J., Wang, L., Fan, A., Wang, J., Xu, B., Jacob, T. J., and Chen, L. (2007) Blockage of volume-activated chloride channels inhibits migration of nasopharyngeal carcinoma cells. *Cell. Physiol. Biochem. 19*, 249−258.

(26) Kanzawa, T., Germano, I. M., Kondo, Y., Ito, H., Kyo, S., and Kondo, S. (2003) Inhibition of telomerase activity in malignant glioma cells correlates with their sensitivity to Temozolomide. *Br. J. Cancer 89*, 922−929.

(27) Cheng, Y., Sk, U. H., Zhang, Y., Ren, X. C., Zhang, L., Huber-Keener, K. J., Sun, Y. W., Liao, J., Amin, S., Sharma, A. K., and Yang, J. M. (2012) Rational Incorporation of Selenium into Temozolomide Elicits Superior Antitumor Activity Associated with Both Apoptotic and Autophagic Cell Death. *PLoS One 7*, e35104.

(28) Cho, H. Y., Wang, W. J., Jhaveri, N., Torres, S., Tseng, J., Leong, M. N., Lee, D. J., Goldkorn, A., Xu, T., Petasis, N. A., Louie, S. G., Schonthal, A. H., Hofman, F. M., and Chen, T. C. (2012) Perillyl Alcohol for the Treatment of Temozolomide-Resistant Gliomas. *Mol. Cancer Ther. 11*, 2462−2472.

(29) Ryu, C. H., Yoon, W. S., Park, K. Y., Kim, S. M., Lim, J. Y., Woo, J. S., Jeong, C. H., Hou, Y., and Jeun, S. S. (2012) Valproic acid

DOI: 10.1021/acschemneuro.5b00178
ACS Chem. Neurosci. 2016, 7, 275−285

downregulates the expression of MGMT and sensitizes Temozolomide-resistant glioma cells. *J. Biomed. Biotechnol. 2012*, 987495.
(30) Wu, Q., Chang, Y., Zhang, L., Zhang, Y., Tian, T., Feng, G., Zhou, S., Zheng, Q., Han, F., and Huang, F. (2013) SRPK1 Dissimilarly Impacts on the Growth, Metastasis, Chemosensitivity and Angiogenesis of Glioma in Normoxic and Hypoxic Conditions. *J. Cancer 4*, 727−735.
(31) Chen, L. X., Zhu, L. Y., Jacob, T. J., and Wang, L. W. (2007) Roles of volume-activated Cl- currents and regulatory volume decrease in the cell cycle and proliferation in nasopharyngeal carcinoma cells. *Cell Proliferation 40*, 253−267.
(32) Huang, W., Liu, M., Zhu, L., Liu, S., Luo, H., Ma, L., Wang, H., Lu, R., Sun, X., Chen, L., and Wang, L. (2014) Functional expression of chloride channels and their roles in the cell cycle and cell proliferation in highly differentiated nasopharyngeal carcinoma cells. *Physiol. Rep. 2*, e12137.
(33) Roos, W. P., and Kaina, B. (2006) DNA damage-induced cell death by apoptosis. *Trends Mol. Med. 12*, 440−450.
(34) Olive, P. L., and Banath, J. P. (2006) The comet assay: a method to measure DNA damage in individual cells. *Nat. Protoc. 1*, 23−29.
(35) Moller, P., Knudsen, L. E., Loft, S., and Wallin, H. (2000) The comet assay as a rapid test in biomonitoring occupational exposure to DNA-damaging agents and effect of confounding factors. *Cancer Epidemiol., Biomarkers Prev. 9*, 1005−1015.
(36) Liao, W., McNutt, M. A., and Zhu, W. G. (2009) The comet assay: a sensitive method for detecting DNA damage in individual cells. *Methods 48*, 46−53.
(37) Ballesta, A., Zhou, Q., Zhang, X., Lv, H., and Gallo, J. M. (2014) Multiscale design of cell-type-specific pharmacokinetic/pharmacodynamic models for personalized medicine: application to Temozolomide in brain tumors. *CPT: Pharmacometrics Syst. Pharmacol. 3*, e112.
(38) Andrasi, M., Bustos, R., Gaspar, A., Gomez, F. A., and Klekner, A. (2010) Analysis and stability study of Temozolomide using capillary electrophoresis. *J. Chromatogr. B: Anal. Technol. Biomed. Life Sci. 878*, 1801−1808.
(39) Wick, W., Wick, A., Schulz, J. B., Dichgans, J., Rodemann, H. P., and Weller, M. (2002) Prevention of irradiation-induced glioma cell invasion by Temozolomide involves caspase 3 activity and cleavage of focal adhesion kinase. *Cancer Res. 62*, 1915−1919.
(40) Han, S., Li, Z., Master, L. M., Master, Z. W., and Wu, A. (2014) Exogenous IGFBP-2 promotes proliferation, invasion, and chemoresistance to Temozolomide in glioma cells via the integrin beta1-ERK pathway. *Br. J. Cancer 111*, 1400−1409.
(41) Gunther, W., Pawlak, E., Damasceno, R., Arnold, H., and Terzis, A. J. (2003) Temozolomide induces apoptosis and senescence in glioma cells cultured as multicellular spheroids. *Br. J. Cancer 88*, 463−469.
(42) Jaracz, S., Chen, J., Kuznetsova, L. V., and Ojima, I. (2005) Recent advances in tumor-targeting anticancer drug conjugates. *Bioorg. Med. Chem. 13*, 5043−5054.
(43) Allen, T. M. (2002) Ligand-targeted therapeutics in anticancer therapy. *Nat. Rev. Cancer 2*, 750−763.
(44) Arrowsmith, J., Jennings, S. A., Clark, A. S., and Stevens, M. F. (2002) Antitumor imidazotetrazines. 41. Conjugation of the antitumor agents mitozolomide and Temozolomide to peptides and lexitropsins bearing DNA major and minor groove-binding structural motifs. *J. Med. Chem. 45*, 5458−5470.
(45) Pipkorn, R., Waldeck, W., Didinger, B., Koch, M., Mueller, G., Wiessler, M., and Braun, K. (2009) Inverse-electron-demand Diels-Alder reaction as a highly efficient chemoselective ligation procedure: Synthesis and function of a BioShuttle for Temozolomide transport into prostate cancer cells. *J. Pept. Sci. 15*, 235−241.
(46) Chen, T. C., Cho, H. Y., Wang, W., Barath, M., Sharma, N., Hofman, F. M., and Schonthal, A. H. (2014) A novel Temozolomide-perillyl alcohol conjugate exhibits superior activity against breast cancer cells in vitro and intracranial triple-negative tumor growth in vivo. *Mol. Cancer Ther. 13*, 1181−1193.
(47) Li, R., Tang, D., Zhang, J., Wu, J., Wang, L., and Dong, J. (2014) The Temozolomide derivative 2T-P400 inhibits glioma growth via administration route of intravenous injection. *J. Neuro-Oncol. 116*, 25−30.
(48) Watkins, S., and Sontheimer, H. (2011) Hydrodynamic cellular volume changes enable glioma cell invasion. *J. Neurosci. 31*, 17250−17259.
(49) Bady, P., Diserens, A. C., Castella, V., Kalt, S., Heinimann, K., Hamou, M. F., Delorenzi, M., and Hegi, M. E. (2012) DNA fingerprinting of glioma cell lines and considerations on similarity measurements. *Neuro-Oncol. 14*, 701−711.

DOI: 10.1021/acschemneuro.5b00178
ACS Chem. Neurosci. 2016, 7, 275−285